SAND2013-10240C

THE BENEFITS OF ENERGY STORAGE COMBINED WITH HVDC TRANSMISSION POWER MODULATION FOR MITIGATING INTER-AREA OSCILLATIONS

J. Neely[1], R. Elliott[1], R. Byrne[1], D. Schoenwald[1], D. Trudnowski[2], M. Donnelly[2]
[1]Sandia National Laboratories, Albuquerque, NM 87123
[2]Department of Electrical Engineering, Montana Tech University, Butte, Montana 59701

The modern power grid is a complex and dynamic system that relies on both distributed and centralized controls. When large generation and load complexes are separated by long transmission lines, the propensity for complex inter-area oscillations increases. These oscillations have been identified as a hazard for utility systems since they may cause damage to equipment or restrictions on power flows over select transmission lines. In previous work, active damping methods have been investigated that include power modulation between areas using energy storage or high voltage dc transmission (HVDC). More recently, the latter approach has been pursued in the western interconnection due to the availability of existing infrastructure, specifically the Pacific DC Intertie (PDCI). Unfortunately, the HVDC damping scheme only allows the modulation of power between two buses, providing limited controllability over certain oscillatory modes, such as those oriented more or less perpendicular to the PDCI. In this paper, the benefits of adding additional energy storage to improve controllability are highlighted through analysis and simulation, including an official base case for the western North American Power System (wNAPS).

Keywords: wNAPS, damping control, PDCI, inter-area oscillations

INTRODUCTION

Damping of inter-area oscillations in the western North American power system (wNAPS) has been the subject of research and development for over three decades. Several approaches have been considered, including tuning of power system stabilizers using a local frequency measurement, modulation of static VAR compensators for damping control [1]-[2], thyristor braking [3] and series impedance modulation [4].

Most recently, there has been increased attention on the use of Pacific DC Intertie (PDCI) modulation and/or energy storage based damping controllers that modulate power at two locations [5],[6]. The PDCI modulates power flow between the Celilo plant in northern Oregon and Sylmar in Southern California. Based on previous work, there is strong evidence that this system will be effective at damping inter-area oscillations if a component of power modulation is a function of the difference in measured frequencies at the two locations. In addition, by utilizing existing PDCI infrastructure, the cost of expensive energy storage hardware is avoided. Unfortunately, this transmission system is static; it cannot be easily adjusted later to improve damping control. In addition, aside from electrical losses, the power sourced/sinked at Celilo is roughly equal to that sinked/sourced at Sylmar. In contrast, the location of energy storage based damping controllers is flexible and control gains can be adjusted separately at each installation; however, investigations have thus far focused on pairs of nodes with equal and opposite power modulation.

In this paper, we consider a damping control scheme that includes HVDC and energy storage based components, thus allowing for power to be modulated at more than two areas. In particular, a three node approach is considered herein and shown to provide superior controllability of certain oscillatory modes. The value of having greater than two nodes is illustrated using two simple Matlab simulation examples, and a practical implementation is investigated through simulation of a Western Electric Coordinating Council (WECC) developed base case (using General Electric's Positive Sequence Load Flow (PSLF) simulation software).

BACKGROUND

In this section, background is provided on inter-area oscillations in the wNAPS, and an introductory model is given with respect to a two-area system.

Inter-Area Oscillations

Inter-area modes are described by frequency and shape. Several low frequency oscillation modes in the wNAPS have been identified, including [7]

- "North-South A" mode, nominally near 0.25 Hz
- "North-South B" mode, nominally near 0.4 Hz
- "East-West" mode, nominally near 0.5 Hz;
- "BC" mode, nominally near 0.6 Hz;
- "Montana" mode, nominally near 0.8 Hz

After a stimulus to the system, mode shape is determined by observing the phase relationship between generators at the specified frequency [8]. Figure 1 illustrates the mode shape for the "North-South B" mode in the wNAPS, shown here at 0.37 Hz, as determined through simulation using a numerical simulation package called Positive Sequence Load Flow (PSLF). The red and purple dots indicate key generators that are oscillating against one another. As can be seen in the map, generators in the northwest US and British Columbia are oscillating against generators in the southwest US and Alberta.

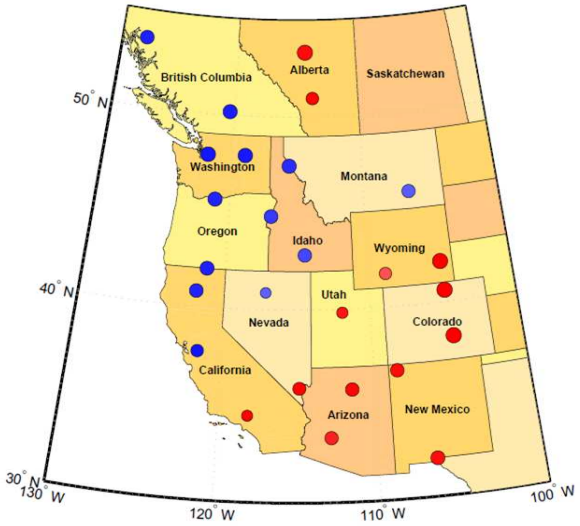

Figure 1: North-South B mode shape in the wNAPS; **red** and **purple** dots are out of phase; diameter indicates amplitude of oscillation

Two-Area System Example

In much of the literature, discussion and analysis of inter-area oscillations is presented first using a two-area system. A simple formulation is presented here.

For a linearized composite power system model, each area is modeled by a collective inertia *M* and a damping coefficient *D* and a tie-line is included linking the two areas [9]. The resulting small-signal dynamics of a two area system with transmission are modeled here by the following fourth-order system

$$\frac{d}{dt}\begin{bmatrix}\Delta\omega_1\\ \Delta\delta_1\\ \Delta\omega_2\\ \Delta\delta_2\end{bmatrix}=\begin{bmatrix}\frac{-D_1}{M_1} & \frac{-T_{12}}{M_1} & 0 & \frac{T_{12}}{M_1}\\ 1 & 0 & 0 & 0\\ 0 & \frac{T_{12}}{M_2} & \frac{-D_2}{M_2} & \frac{-T_{12}}{M_2}\\ 0 & 0 & 1 & 0\end{bmatrix}\begin{bmatrix}\Delta\omega_1\\ \Delta\delta_1\\ \Delta\omega_2\\ \Delta\delta_2\end{bmatrix}+\begin{bmatrix}\frac{1}{M_1} & 0\\ 0 & 0\\ 0 & \frac{1}{M_2}\\ 0 & 0\end{bmatrix}\begin{bmatrix}\Delta P_1\\ \Delta P_2\end{bmatrix} \quad (1)$$

where $\Delta\omega_1, \Delta\omega_2$ are the collective generator speed deviations from nominal for areas 1 and 2, M_1, M_2 are the area inertia constants, D_1, D_2 are the damping coefficients, $\Delta P_1, \Delta P_2$ are deviations in power balance (generation minus load) and T_{12} is the synchronizing torque coefficient identified at the specified operating point and defined as follows [9]

$$T_{12}=\frac{V_1 V_2 \cos(\delta_{10}-\delta_{20})}{X_{12}} \quad (2)$$

where X_{12} is the impedance of the transmission line connecting the two areas, V_1, V_2 are the line voltages of the two buses and δ_{10}, δ_{20} are the relative rotor angle at the specified operating point. It is noted in this model that M_1, M_2 have units of seconds, δ_{10}, δ_{20} are in radians and all other quantities are in *per unit*.

Equation (1) has the familiar linear system form $\dot{x}=Ax+Bu$ where $x=[\Delta\omega_1 \quad \Delta\delta_1 \quad \Delta\omega_2 \quad \Delta\delta_2]^T$ is the system state and the inputs $u=[\Delta P_1 \quad \Delta P_2]^T$ act as disturbances to the system, and the response of the system to these disturbances is governed primarily by the eigenvalues of the A matrix. It is noted that this model is greatly simplified and used here only for illustrative purposes and does not include models for certain elements necessary to a practical system, such as droop control and speed governing.

To aid in visualizing the linked dynamical response of the two areas, it is helpful to consider, as an analogy, a pair of mass-spring-damper systems linked by a spring between the two masses. See Figure 2. The force of the spring between the two masses works to align the position of the two masses just as synchronizing torque works to synchronize electrical angle (and thus rotor positions). The green arrows are indicative of corrective forces that might be applied by an external regulator, such as a damping control system.

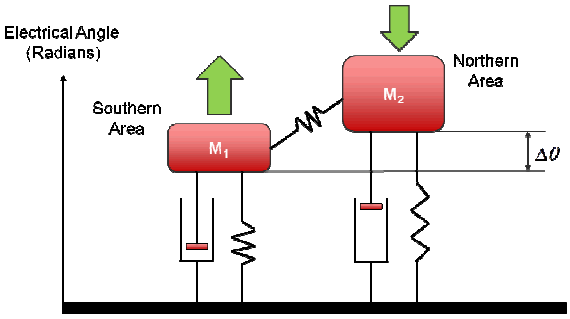

Figure 2: Oscillations in a two-area system may be visualized as oscillations in two mass-spring-damper systems

ACTIVE DAMPING USING POWER MODULATION

In this section, damping control schemes based on energy storage and HVDC power modulation are presented.

Damping Controller based on Energy Storage

To mitigate the severity of inter-area oscillations, a damping control scheme has been proposed that modulates real power at key buses in each area based on the difference in frequency sensed in each area. Specifically, information about each area frequency is transmitted to the local controller and the controller in the other area. See Figure 3 [6].

Using an energy storage system capable of sourcing or sinking power, the power delivered to the respective bus is given by the following

$$P_{d1}=-K_d\left(f_1(t)-f_2\left(t-T_{delay}\right)\right) \quad (3)$$

$$P_{d2} = -K_d\left(f_2(t) - f_1\left(t - T_{delay}\right)\right) \quad (4)$$

where P_{d1}, P_{d2} are the powers delivered by the respective damping controllers in megawatts (MW), K_d is the damping gain, often designated in MW/Hz or MW/mHz, f_1, f_2 are the system frequencies in Hz and T_{delay} is the network latency (in seconds) [6]. In this implementation, the local frequency is attained through local measurement at the point of common coupling.

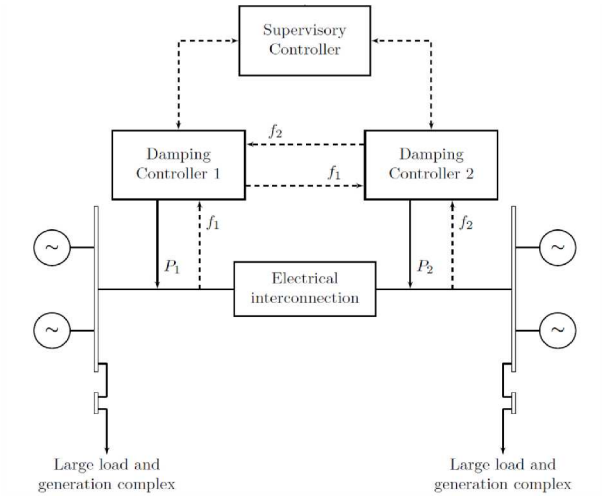

Figure 3: Energy storage based damping controller architecture for two-area system

To incorporate this control into the model of (1), the damping gain must instead be represented in per unit. In addition, it is convenient to neglect the time delay for clarity. Thus, neglecting time delay and designating the per unitized damping gain as $\overline{K}_d$, the damping controller may be incorporated into (1) as follows

$$\frac{d}{dt}\begin{bmatrix}\Delta\omega_1\\ \Delta\delta_1\\ \Delta\omega_2\\ \Delta\delta_2\end{bmatrix} = \begin{bmatrix}\frac{-D_1-\overline{K}_d}{M_1} & \frac{-T_{12}}{M_1} & \frac{\overline{K}_d}{M_1} & \frac{T_{12}}{M_1}\\ 1 & 0 & 0 & 0\\ \frac{\overline{K}_d}{M_2} & \frac{T_{12}}{M_2} & \frac{-D_2-\overline{K}_d}{M_2} & \frac{-T_{12}}{M_2}\\ 0 & 0 & 1 & 0\end{bmatrix}\begin{bmatrix}\Delta\omega_1\\ \Delta\delta_1\\ \Delta\omega_2\\ \Delta\delta_2\end{bmatrix} + \begin{bmatrix}\frac{1}{M_1} & 0\\ 0 & 0\\ 0 & \frac{1}{M_2}\\ 0 & 0\end{bmatrix}\begin{bmatrix}\Delta P_1\\ \Delta P_2\end{bmatrix} \quad (5)$$

For an exemplary system with parameters given in Table 1, Figure 4 illustrates the effect of $\overline{K}_d$ on the poles of the system defined by (5). Specifically, oscillatory modes are indicated by pole-pairs with imaginary components. The damping coefficient of the mode is greater for pole-pairs having more negative real-valued components in relation to the imaginary component. In this example, $\overline{K}_d$ is increased from 0.0 to 0.50 per unit, causing the poles to move left in the imaginary plane (more negative real parts), which indicates increased damping.

Table 1. Parameters used for Two-Area Example

Description	Parameter	Value
Area inertias	$M_1 = M_2$	6 sec
Area damping coefficients	$D_1 = D_2$	1.2
Synchronizing Torque Coefficient	T_{12}	3.132
Damping Gain	$\overline{K}_d$	0.0-0.5

To demonstrate the effect of the damping controller on the time-domain response, the system described by (5) and Table 1 was simulated for different $\overline{K}_d$ values using the Matlab ode solver *ode45*. Specifically, at *t*=5 seconds, ΔP_1 was stepped from 0.0 to -0.01 and then back down to 0.0 at t=7. This represents a momentary 1% increase in load. The result is a *ring-down* event shown in Figure 5; therein, the units are given in mHz. Without damping, $\overline{K}_d = 0$, the inter-area oscillation magnitude is above 25 mHz for 20 seconds after the stimulus. With the damping control at $\overline{K}_d = 0.5$, the oscillations decay more quickly and the amplitude does not rise above 25 mHz beyond 10 seconds following the stimulus.

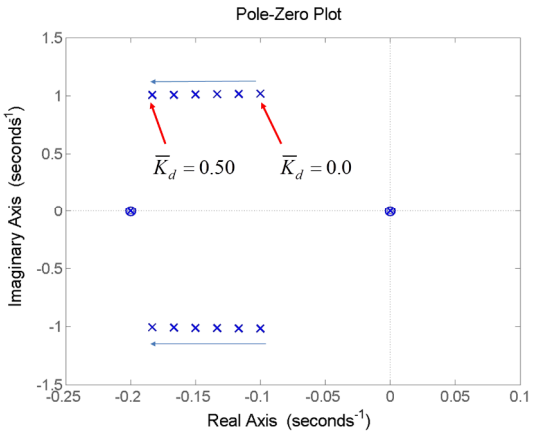

Figure 4: Eigenvalues for example two-area system with $\overline{K}_d$ increasing from 0.0 to 0.50 per unit.

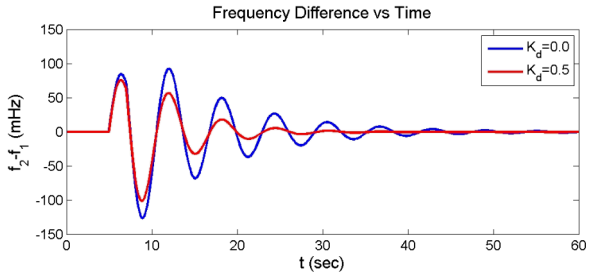

Figure 5: Time domain simulation of two-area model, showing effect of damping on inter-area oscillation

Damping Controller based on HVDC Transmission

The approach employed in HVDC transmission is similar in principle to that presented for energy storage. To mitigate inter-area oscillations, an additional power flow is computed as a function of the difference in frequency between the two areas and superimposed onto the scheduled power flow. In particular, the Pacific DC Inter-tie (PDCI) is an existing HVDC system with a high capacity, and it is currently being investigated for damping control.

There are three distinguishing limitations to HVDC based damping control; these include

(1) Power flow can only be modulated between two nodes
(2) The power flow must be symmetrical (aside from the effect of transmission efficiency)
(3) There are a limited number of existing systems to exploit for damping applications

Using an HVDC transmission system, the power delivered to the respective bus is given by the following

$$P_{d1} = -K_d\left(f_1\left(t - T_{delay1}\right) - f_2\left(t - T_{delay2}\right)\right) \quad (6)$$

$$P_{d2} = -K_d\eta_{HVDC}\left(f_2\left(t - T_{delay2}\right) - f_1\left(t - T_{delay1}\right)\right) \quad (7)$$

where the static power flow is defined from bus 1 to bus 2, $\eta_{HVDC} < 1$ is the efficiency, and the controller attains frequency information from each bus over a network with latencies T_{delay1} and T_{delay2} (in seconds) respectively.

DAMPING OF MULTIPLE AREAS

As illustrated in the previous section, inter-area oscillations can be mitigated through the addition of a two-node damping control system that modulates power in each area in response to the difference in frequency (or generator speed). This approach is straight forward when there are two areas oscillating against one another. As will be illustrated here, with a simple three-area example, a two-node implementation can be insufficient in some scenarios as it can lack controllability of an oscillatory mode.

Three-Area System Example

The system presented in (1) is easily expanded to represent a three area system. In this case, there are three inertias, three damping coefficients and three tie-lines connecting the three areas. In this implementation, two feedback gains are used $\overline{K}_{d1}$ and $\overline{K}_{d2}$. The gain $\overline{K}_{d1}$ specifies the damping gain between areas 1 and 2 while $\overline{K}_{d2}$ specifies a control effort only in area 3 in relation to 1 and 2. The resulting system model is given by $\dot{x} = Ax + Bu$ with inputs $u = \left[\Delta P_1 \quad \Delta P_2 \quad \Delta P_3\right]^T$ state $x = \left[\Delta\omega_1 \quad \Delta\delta_1 \quad \Delta\omega_2 \quad \Delta\delta_2 \quad \Delta\omega_3 \quad \Delta\delta_3\right]^T$ and A and B matrices given by (8) and (9). All parameters are defined in Table 2.

$$A = \begin{bmatrix} \frac{-D_1 - K_{d1}}{M_1} & \frac{-T_{12} - T_{13}}{M_1} & \frac{K_{d1}}{M_1} & \frac{T_{12}}{M_1} & 0 & \frac{T_{13}}{M_1} \\ 1 & 0 & 0 & 0 & 0 & 0 \\ \frac{K_{d1}}{M_2} & \frac{T_{12}}{M_2} & \frac{-D_2 - K_{d1}}{M_2} & \frac{-T_{12} - T_{23}}{M_2} & 0 & \frac{T_{23}}{M_2} \\ 0 & 0 & 1 & 0 & 0 & 0 \\ \frac{K_{d2}}{2M_3} & \frac{T_{13}}{M_3} & \frac{K_{d2}}{2M_3} & \frac{T_{23}}{M_3} & \frac{-D_3 - K_{d2}}{M_3} & \frac{-T_{13} - T_{23}}{M_3} \\ 0 & 0 & 0 & 0 & 1 & 0 \end{bmatrix} \quad (8)$$

$$B = \begin{bmatrix} \frac{1}{M_1} & 0 & 0 \\ 0 & 0 & 0 \\ 0 & \frac{1}{M_2} & 0 \\ 0 & 0 & 0 \\ 0 & 0 & \frac{1}{M_3} \\ 0 & 0 & 0 \end{bmatrix} \quad (9)$$

Table 2. Parameters used for Three-Area Example

Description	Parameter	Value
Area inertias	$M_1 = M_2$	6 sec
-	M_3	7 sec
Area damping coefficients	$D_1 = D_2$	1.2
-	D_3	1.0
Synchronizing Torque Coefficients	T_{12}	3.929
-	T_{13}	3.297
-	T_{23}	2.498
Damping Gains	$\overline{K}_{d1}$	0.0-0.5
-	$\overline{K}_{d2}$	0.0-1.0

Figures 6 and 7 show a pole-zero plots as the respective gains are adjusted; therein two oscillatory modes are seen close in frequency. As $\overline{K}_{d1}$ is increased, only one pair of poles moves to the left; the other pair is not greatly affected. Likewise, as $\overline{K}_{d2}$ is increased, the second pole-pair is damped, but the first is not affected. This is further investigated through time-domain simulation as in the two-area example. Area 1 is stimulated by the same disturbance applied to ΔP_1 as in the previous example and the differences in area frequencies are observed in Figures 8 and 9.

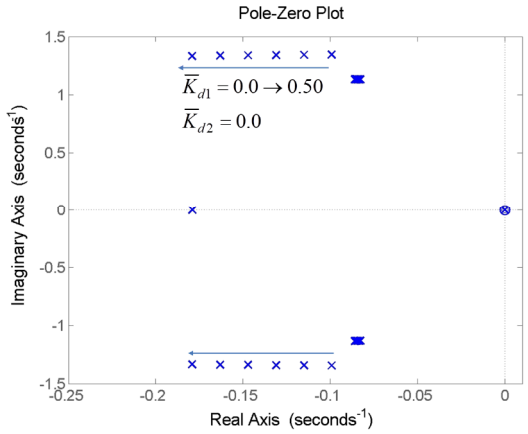

Figure 6: Eigenvalues for example three-area system with $\overline{K}_{d1}$ increasing from 0.0 to 0.50 per unit.

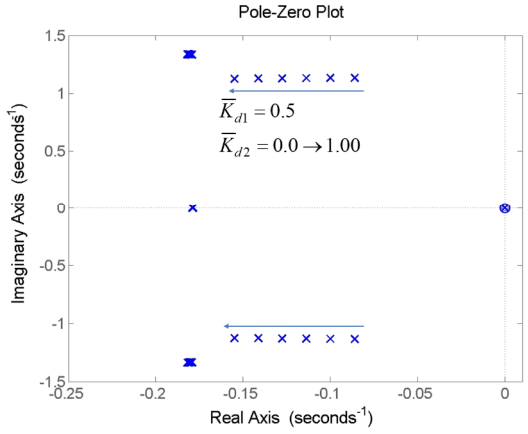

Figure 7: Eigenvalues for example three-area system with $\overline{K}_{d2}$ increasing from 0.0 to 1.0 per unit.

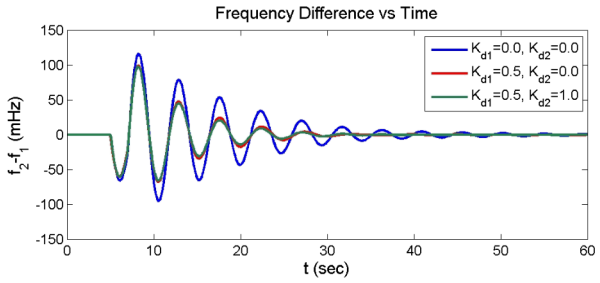

Figure 8: Time domain simulation of three-area model, showing effect of damping on different oscillatory mode

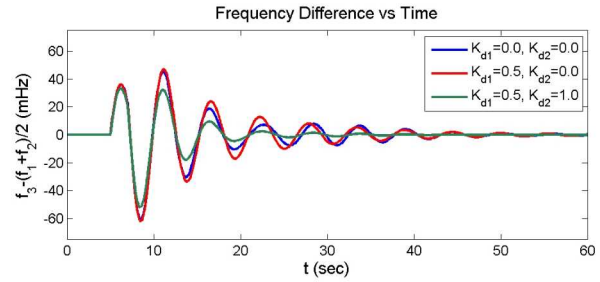

Figure 9: Time domain simulation of three-area model, showing effect of damping on different oscillatory modes

In particular, as $\overline{K}_{d1}$ is increase from 0.0 to 0.5, one sees in Figure 8 that the oscillation between area 1 and area 2 is decreased. Counter-intuitively, one sees in Figure 9 that the oscillation between area 3 and the rest of the system appears initially to get slightly larger in amplitude; though, it does not appear to decay any faster after the first 2 cycles. This is believed to be due to interference between the two modes which are close in frequency. As the first mode is damped out, it no longer interferes with the second mode, and the amplitude appears slightly larger just after the stimulus. As $\overline{K}_{d2}$ is increased, it is seen in Figure 9 that the oscillation between area 3 and the rest of the system is now reduced, but there is little additional reduction to the oscillation between areas 1 and 2.

The above results indicate a controllability issue and suggest that damping between area-pairs may be insufficient to address all the oscillatory modes in a practical system.

SIMULATION RESULTS IN PSLF

In this section, a three-node damping control scheme that utilizes both the PDCI and energy storage is applied to a dynamic model developed by the Western Electric Coordinating Council (WECC) to represent a scenario in the western North American Power System (wNAPS). Specifically, a WECC-developed base case representing a lightly-loaded wNAPS in Spring 2022 was considered. In this model, the PDCI power flow was directed from Celilo to Sylmar. For this study, the model was augmented to include PDCI damping as well as an energy storage damping node in Ault (near Denver). See Figure 10. In this configuration, the dynamics of the grid are believed to behave similar to that of the three-area system described earlier. These areas are encircled in Figure 10 in the North around Celilo, the South around Sylmar and in the East around Ault.

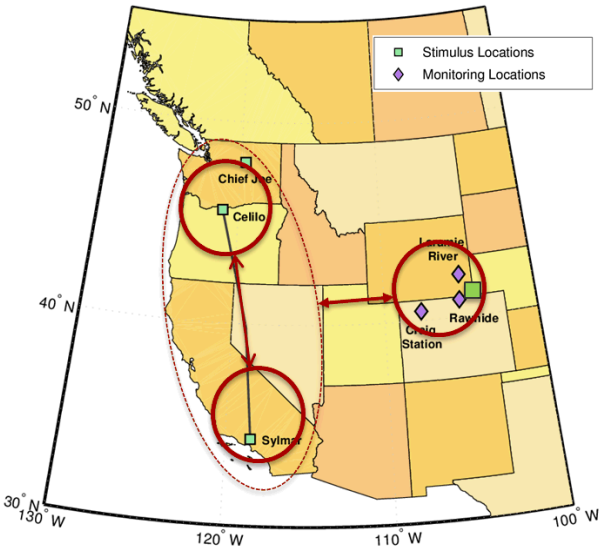

Figure 10: Map of the wNAPS with key locations indicated for this study

To further illustrate the damping control scheme, the mass-spring-damper system analogy is extended here to represent a three-area system; see Figure 11.

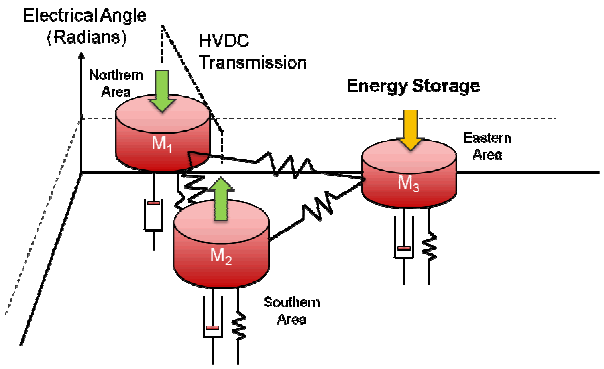

Figure 11: The mass-spring-damper analogy is extended in this illustration to a three-area system

The power delivered by the damping control nodes in this study is equivalent to the following

$$\begin{bmatrix} P_1 \\ P_2 \\ P_3 \end{bmatrix} = \begin{bmatrix} -K_{d1} & K_{d1} & 0 \\ K_{d1}\eta_{PDCI} & -K_{d1}\eta_{PDCI} & 0 \\ \frac{K_{d2}}{2} & \frac{K_{d2}}{2} & -K_{d2} \end{bmatrix} \begin{bmatrix} f_1 \\ f_2 \\ f_3 \end{bmatrix} \quad (10)$$

where $\eta_{PDCI} \approx 0.91$ is the efficiency of the PDCI transmission circuit, K_{d1} is the damping gain applied to the PDCI and K_{d2} is the damping gain applied to the energy storage unit in Ault. In this study, the sets of gains were considered:

- No damping: $K_{d1} = 0, K_{d2} = 0$ MW/mHz
- PDCI damping: $K_{d1} = 6, K_{d2} = 0$ MW/mHz
- PDCI & ES damping: $K_{d1} = 6, K_{d2} = 6$ MW/mHz

For each case, the system was simulated using Positive Sequence Load Flow (PSLF) for 30 seconds. At *t*=5 sec, an oscillatory response was stimulated using the *Chief Joseph Brake* in Washington, which provides an momentary increase in load and stimulates a ring down response in the grid model.

As in the three-area model described earlier, the WECC model has distinct modes; in this case, these are believed to be primarily composed of the North-South B mode and the East-West mode. For this paper, these modes are visualized by analyzing speed differences between generators. In this study, the East-West mode is observed by looking at the speed difference between the average of Raw Hide and Craig Station and the average of Palo Verde and John Day. The North-South modes is observed by looking at the difference between Palo Verde and John Day.

When K_{d1} is increased from 0 to 6 MW/mHz, Figure 13 shows that the PDCI-based scheme dampens the North-South B oscillation. However, Figure 14 indicates that the East-West mode appears to oscillate with greater amplitude than in the *no damping* case. However, when the energy storage damping control is engaged, by increasing K_{d2} from 0 to 6 MW/mHz, the ring-down responses indicate improvement in damping the East-West mode using the third energy storage damping node.

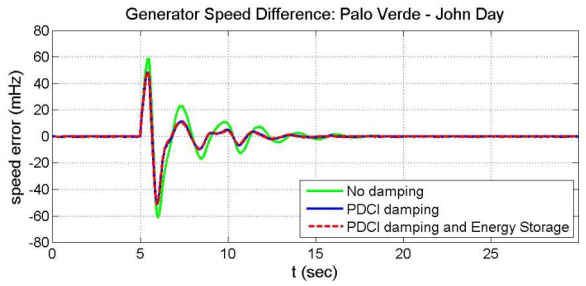

Figure 13: Time domain simulation of WECC-developed model, showing effect of damping on North-South mode

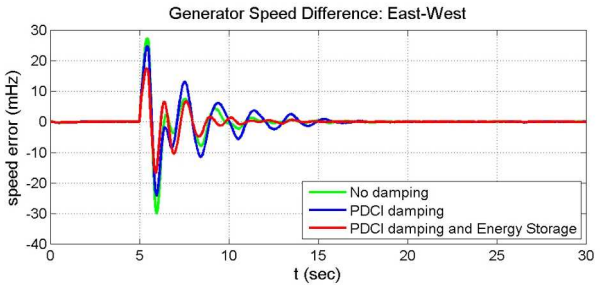

Figure 14: Time domain simulation of WECC-developed model, showing effect of damping on East-West mode

To illustrate the value of the additional energy storage node, two generator speed errors, for Raw Hide and Craig Station, are shown in Figure 15. These errors in generator speed indicate additional stresses on equipment in response to a stimulus thousands of miles away in the grid. With PDCI-based damping, the oscillations actually increase in amplitude, which defeats the purpose of the control. However, with the additional energy storage node, the generator response is greatly mitigated.

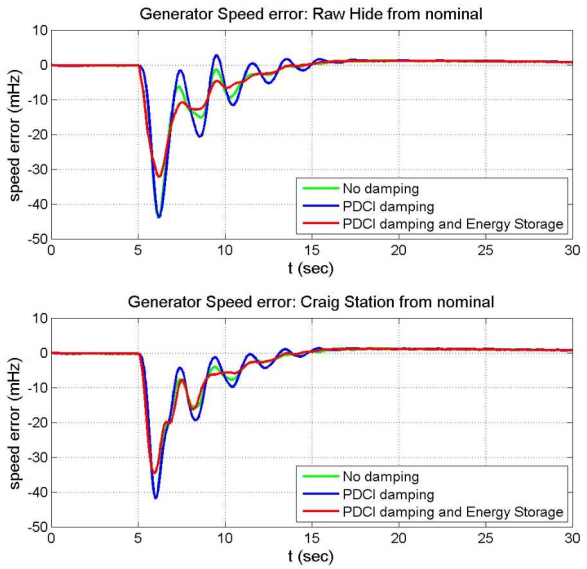

Figure 15: Time domain simulation of WECC-developed model, showing effect of damping on select generator speed errors

In this 2022 basecase, much of the conventional generation has been displaced by renewables reducing system inertia and thus reducing the frequency of certain modes. In this case, the North-South B mode

and East-West mode are closer in frequency than the nominal values, and it is believed that they are interfering destructively. When the PDCI damps the North-South B mode, the East-West mode is better expressed in the time domain. However, the energy storage based damping control has greater controllability of the East-West mode; engaging it along with the PDCI-based approach allows both modes to mitigated.

CONCLUSIONS

In this paper, the benefits of using both energy storage and high voltage DC transmission have been discussed. In particular, the PDCI has recently been considered for implementing damping control. The approach exploits existing infrastructure, but the PDCI is static and only modulates power between a pair of nodes. This system may not allow adequate damping of all oscillatory modes. Through the use of additional energy storage nodes, a multi-node damping control scheme may be realized to improve damping of several modes. The benefits are illustrated herein using Matlab simulations, and the applicability of the approach is demonstrated through simulation of the wNAPS in PSLF.

FUTURE WORK

In future work, a more generalized analysis will be developed for formulating the damping control system as a multiple input multiple output (MIMO) system. Using this formulation, control gains may be determined optimally using methods similar to quadratic regulator control design. In particular, preliminary results of this approach reveal that symmetrical power modulations, and thus symmetrical gains, are in fact not indicated unless the corresponding inertias and damping coefficients of the areas are identical.

Finally, implementations will be investigated that include HVDC and energy storage co-located at a single node. This approach would allow for unsymmetrical modulation (different gains at each end of the HVDC) while utilizing existing infrastructure and thus minimizing the size of the energy storage hardware needed.

ACKNOWLEDGMENT

The authors would like to acknowledge the support of: Dr. Imre Gyuk, DOE Energy Storage Program; Phil Overholt, DOE Transmission Reliability Program; and the BPA Technology Innovation Program (Dr. Dmitry Kosterev, POC).

Sandia National Laboratories is a multi-program laboratory managed and operated by Sandia Corporation, a wholly owned subsidiary of Lockheed Martin Corporation, for the U.S. Department of Energy's National Nuclear Security Administration under contract DE-AC04-94AL85000.

References

[1] J.Quintero and V.M.Venkatasubramanian, “A real-time wide-area control framework for mitigating small-signal instability in large electric power systems,” in Proceedings of the 38th Hawaii International Conference on System Sciences, pp. 66–75, January 2005.

[2] J.Q.Restrepo, *A Real-Time Wide-Area Control for Mitigating Small-Signal Instability in Large Electric Power Systems*. PhD thesis, Washington State University, May 2005.

[3] THYRISTOR BRAKING REFERENCE

[4] Chakrabortty, A., "Wide-area damping control of power systems using clustering and FACTS-based redesigns," *American Control Conference (ACC), 2012* , pp.4446,4451, 27-29 June 2012.

[5] J. Undrill, “Investigation of asymptotic stability of low frequency oscillations,” tech. rep., Report to Bonneville Power Administration, Portland, OR, 2010.

[6] Neely, J.C.; Byrne, R.H.; Elliott, R.T.; Silva-Monroy, C. A.; Schoenwald, D.A.; Trudnowski, D.J.; Donnelly, M.K., "Damping of inter-area oscillations using energy storage," *Power and Energy Society General Meeting (PES), 2013 IEEE* , 21-25 July 2013.

[7] D. Trudnowski, “Baseline Damping Estimates,” Report to Bonneville Power Administration, September 2008.

[8] Trudnowski, D.J., "Estimating Electromechanical Mode Shape From Synchrophasor Measurements," *Power Systems, IEEE Transactions on* , vol. 23, no.3, pp.1188,1195, Aug. 2008.

[9] P. Kundur, Power System Stability and Control. New York: McGraw-Hill, Inc., 1993.

[10] Inter-Area Oscillations in Power Systems, A Nonlinear and Nonstationary Perspective; Ed. A. R. Messina; Springer; New York, NY; 2009.

[11] D. J. Trudnowski; “Estimating Electromechanical Mode Shape From Synchrophasor Measurements”; IEEE Transactions on Power Systems, vol. 23, no. 3, August 2008.